*Pol. J. Environ. Stud. Vol. 31, No. 6 (2022), 5037-5046*
DOI: *10.15244/pjoes/150643* ONLINE PUBLICATION DATE: 2022-08-30

*Original Research*

# A Study of Erythrocyte Deformation Level Related to Biomass Burning Emission Exposures Using Artificial Neural Networks

**Kasnawi Al Hadi[1,2], Arinto Yudi Ponco Wardoyo[1*], Unggul Pundjung Juswono[1], Agus Naba[1], Arif Budianto[1,2], Eko Teguh Purwito Adi[1]**

[1]Physics Department, Brawijaya University, Jl. Veteran 65145 Malang, East Java, Indonesia
[2]Mataram University, Jl. Majapahit No. 62 83125 Mataram, West Nusa Tenggara, Indonesia

*Received: 25 January 2022*
*Accepted: 2 June 2022*

**Abstract**

Emissions from burning biomass have become a problem in Indonesia. As found on the Indonesian island of Lombok, agricultural waste is burned for traditional industrial activities. On the other hand, biomass burning emissions contain many PMs (particulates) in different size distributions recognized to have a significant correlation to health impact. This study is conducted to predict the impact of the PM exposure on blood using a ANN (artificial neural network) model as well as a histological examination. The relationship between both methods is determined to estimate the impact of biomass burning emissions on the blood. This study used male mice as the experimental animals exposed to PM emissions ($PM_{0.1}$, $PM_{2.5}$, and $PM_{10}$) produced from the burning of various biomass (rice straw, rice husks, corn cobs, corn stalks, and tobacco) taken from Lombok Island. The sample exposure was conducted in a chamber for 100 s for ten sequence days. The blood samples were observed using a microscope with the 400 x magnification. The cell deformation was examined histologically by calculating the normal and abnormal cells. The percentage of the erythrocyte deformation was assessed using a fixed back and forth propagation ANN. The result shows that the biomass burning PM emissions have a significant impact on the erythrocyte deformation depending on the type of biomass and the particulate matter emissions. The ANN model confirms the erythrocyte deformation data obtained by the histological examination method.

**Keywords**: biomass burning, emission, erythrocyte, particulate matter, ANN

*e-mail: a.wardoyo@ub.ac.id

## Introduction

Biomass burning activity is one of the important sources of air pollutants. This activity includes residential wood combustion, mainly for agricultural waste burning [1], forest fire [2], and many others. Many previous studies suggested that air quality impacts of biomass burning emissions vary significantly with the primary sources. These practices refer to many conditions, such as the burning season, biomass types, the frequency of conducting prescribed fires in an area, and the combustion stage, like flaming or smoldering the fire [3-4]. The combustion stage will also influence the emission types. Biomass burning emits many substances, such as organic aerosols or organic particulate matter with certain concentrations [5], particulate-bound PAHs (polycyclic aromatic hydrocarbons) [6], particulate matters (PM), and elemental carbon [7].

PM is air pollution, a mixture of solid particles and liquid droplets suspended in ambient air. According to the diameter size, PMs are classified into $PM_{0.1}$ or ultrafine particles with a diameter ≤0.1 μm [8], fine particles ($PM_{2.5}$) with a diameter ≤2.5 μm [9-10], coarse particles or $PM_{10}$ with a diameter ≤10 μm [11], and TSP (total suspended particles) with a bigger diameter [12]. As studied in an urban area, there is a correlation between deposited fine-mode aerosol and human respiratory tract anomaly [13]. In China, many lung cancer deaths were attributed to $PM_{2.5}$ in 2005, showing $PM_{2.5}$-lung cancer mortality associations [14]. Further investigation confirmed more impacts of $PM_{0.1}$ on human health than other bigger particulate matters [15-16]. Specific to $PM_{0.1}$ and $PM_{2.5}$, some studies examined the deformed erythrocytes and alveolar cells due to motor vehicle emissions exposure, where the deformation levels are dominated in alveolar cells [10, 17-18]. Moreover, an *in vitro* study using mice confirmed that exposure to $PM_{2.5}$ exerts a discernible effect on promoting hepatic fibrogenesis under the normal chow or high-fat diet [19].

The histological method have been mainly used to examine the cell deformations [20-23]. In terms of the deformation level of blood cells was examined histologically by analyzing the observed images [22], and examined the erythrocyte shape using digital imaging from a microscope [21]. The optical examination was also found in investigating erythrocyte deformability in diabetes mellitus cases [23]. These studies have a weakness that they need a longer time for analyzing the images. This method needs a special or trained technician for all procedures [17, 24].

Based on the limitation of the conventional analysis method, there is a need to develop a new method to study the correlation between exposures to PMs and health impact. In this state, ANN (artificial neural networks) can be used to approach the probable correlation or prediction numerically, with a precise prediction result [25]. Compared to the conventional method, such as statistical analysis or manual counting, ANN modeling can improve the data quality and gives satisfactory results [25]. ANN can predict a variable with an optimization algorithm, while the approach gives a reliable way to analyze further parameter with a faster duration [26].

As a novelty, ANN development can be applied for predicting the correlation between PM exposure and the impact in the case of the erythrocyte deformation. For this purposes, this research is conducted to develop an ANN approach for predicting a deformation level. The gold reference for the ANN engine is obtained from the manual counting of the histological examination. The ANN engine is developed using A Levenberg-Marquardt (LM) as the main function due to its ability, hidden neurons, and hidden layers that can be developed as a good ANN engine [27]. The Levenberg-Marquardt training function has a good performance when being used as a feed-forward backpropagation network type [28], with a flexible and optimum layer and neuron number developed for the trained data, whether linear or non-linear approaches [29].

## Materials and Methods

### Measurement System

This study used one hundred and eighty (180) laboratory standard male mice as the experimental animals (purchased from Malang, East Java, Indonesia, bodyweight = 22-23 grams, 20-22 weeks old). These mice were acclimatized for seven consecutive days inside mice cages (relative humidity = 68%, indoor temperature = 25.5ºC) [17, 24]. After that, they were randomly divided into four main groups: control (CTRL), $PM_{0.1}$, $PM_{2.5}$, and $PM_{10}$. Each main group has five subgroups: RS, TB, RH, CR, and CC (Table 1). All animal treatments were under Brawijaya University guidelines for ethical animal use (Ethical clearance code: 541-KEP-UB).

### PM Measurements and Exposures

This study used five different biomass samples obtained from the local area surrounding Lombok Island, Indonesia. They were divided into five codes: RS (rice straw), TB (tobacco), RH (rice husk), CR (corn rod), and CC (corncob). Each biomass sample was weighed (5 grams) and stored in dry packaging with a moisture content ≤10% (natural air-dried). After that, each sample was burned inside a one-way biomass furnace and flowed with air at 4 m/s speed of spray. This speed was chosen according to our preliminary study, in which a faster speed would make the fire burn too big. A lower speed would not make stable combustion. The burning emission was then channeled into a diluter chamber consisting of three filters (Grade 5 (≤2.5 μm) and Grade 2 (≤8 μm) Whatman™ filter

Table 1. Experimental animals grouping.

| Main Group | Subgroup | Total Mice | |
|---|---|---|---|
| CTRL | CTRL1; CTRL2; CTRL2 | n = 10 mice/ subgroup | N = 30 mice |
| $PM_{0.1}$ | RS; TB; RH; CR; CC | n = 10 mice/ subgroup | N = 50 mice |
| $PM_{2.5}$ | RS; TB; RH; CR; CC | n = 10 mice/ subgroup | N = 50 mice |
| $PM_{10}$ | RS; TB; RH; CR; CC | n = 10 mice/ subgroup | N = 50 mice |

papers and $PM_{1.0}$ filters) and a suction pump with a speed of 2 m/s [24]. This chamber was used to measure and expose the mice to the different PM emissions: $PM_{0.1}$, $PM_{2.5}$, and $PM_{10}$. The mice from the $PM_{0.1}$ group were exposed to the $PM_{0.1}$ for 100 seconds emitted by a specific biomass burning as seen in Table 1. These treatments were also applied to other PM groups. Besides, the exposed PMs were measured using a TSI P-Trak Ultrafine Particle Counter ($PM_{0.1}$) and a Hinaway Handheld Air Tester ($PM_{2.5}$ and $PM_{10}$) (Fig. 1) [30]. The exposures were conducted once a day for ten consecutive days.

## Histological Examination

The mice were sacrificed using the cervical disk location method on the 11th day. The blood samples were taken and placed onto object glasses (1.0 mm of thickness). These samples were fixed with methanol solution (70%) and naturally air-dried for five minutes [17, 24]. After that, these samples were colored using Giemsa and buffer pro-Giemsa solution (1:3) and rinsed with aqua dest [24]. These blood samples were observed under a microscope and camera with a magnification of 400x. The number of normal and abnormal (deformed) erythrocytes were counted manually from 25 random fields of view of each mouse (Fig. 2). The deformed cell percentage (*DL*) was calculated using the equation below [20, 24]:

$$DL = \sum Abnormal\ Cells / \sum Cells) \times 100\% \quad (1)$$

## Artificial Neural Networks

ANN with a Levenberg-Marquardt training function was chosen in this study due to the good performance when being used as a feed-forward backpropagation network type [28]. This function also has a flexible and optimum layer and neuron number developed for the trained data, whether linear or non-linear approaches [29] (Eq. (2), Fig. 3). The LM training function was shown by MATLAB2014 software, calculated from $R^2$ value. $R^2$ value shows the data inclination per layer in the ANN engine and determines the best value that can be used as the ANN approach value (deformation level from the ANN engine) [29].

$$R^2 = [\sum y_{ip} - y_{ie}] / [\sum y_{ip} - y_e]^2 \quad (2)$$

The error between the calculated data and approach data (ANN) is shown by an MSE (mean square error) value [29]. MSE can be calculated using equation:

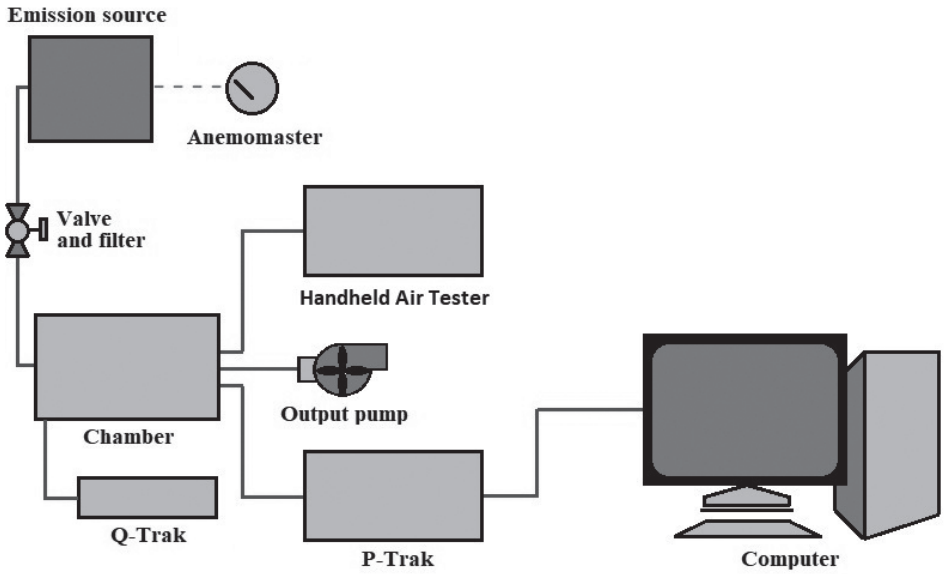


Fig. 1. PM measurement and exposure setup.


Fig. 2. Histological examination under the random fields of view.

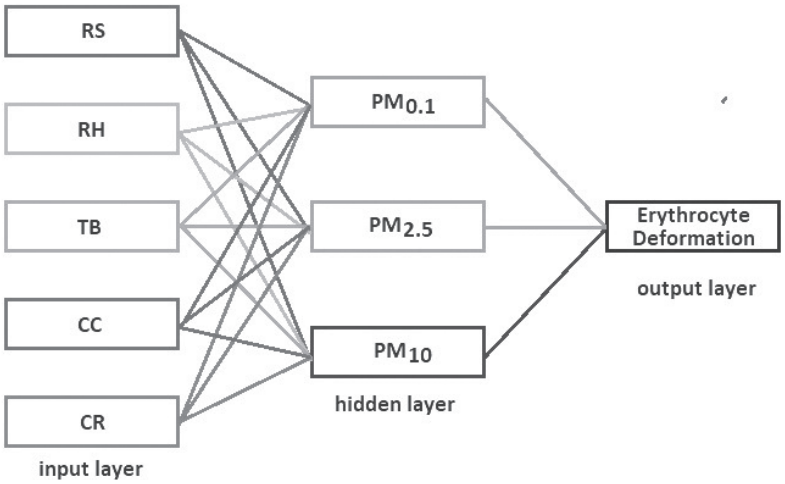


Fig. 3. ANN algorithm schematic.

$$MSE = [\Sigma (y_{ie} - y_{ip})^2 / n ]^{1/2} \quad (3)$$

According to Eq (2-3), the number of experimental data is shown by $n$, while $y_{ip}$ is the prediction value. The experimental data are symbolized by $y_{ie}$.

### Statistical Analysis

Data were presented as the mean value and standard error of the means (SEM). Differences between groups were evaluated using Student's *t*-test. The value of $p<0.05$ was considered to show statistical significance. Linearity constant ($r^2$) was used to test the ANN performance, by comparing the results from ANN approach and manual counting, in which $r^2>0.70$ shows a good linearity [31].

## Results and Discussion

### PM Concentrations

The PM measured concentrations are presented in Table 2. RS dominates the PM concentrations for all. Besides, CR has the smallest $PM_{0.1}$ and $PM_{10}$ concentrations. In $PM_{2.5}$ groups, TB has the smallest $PM_{2.5}$ concentration compared to other biomass samples. According to these measurement results, the highest contributors are rice straw, emitting the most PM concentrations.

Table 2. PM concentrations measured from biomass burning.

| Biomass Samples | PM Concentrations (mean) | | |
|---|---|---|---|
| | $PM_{0.1}$ (pts/cm$^3$) | $PM_{2.5}$ (ug/m$^3$) | $PM_{10}$ (ug/m$^3$) |
| RH | 125,163 | 2,706 | 5,344 |
| RS | 164,733 | 4,445 | 8,040 |
| TB | 93,310 | 2,853 | 6,469 |
| CC | 76,850 | 3,185 | 5,505 |
| CR | 64,287 | 2,830 | 5,405 |

## Erythrocytes Deformation (Manual Counting)

Figs 4-5 shows the deformed cells observed under a digital microscope (400x magnification). More deformed cells are found in the exposed groups compared to the control group. According to the calculation under random fields of view, there are 158 normal erythrocytes found in the control group. Besides, the control group only has 12 deformed cells dominated by helmet-shaped and sickle-shaped cells. Eliptocyte and teardrop-shaped cells are found in a small number.

In order to investigate the most probable factor causing the erythrocyte deformation, we performed the exposures of the PM with different diameters. As shown in Fig. 6, the exposure of $PM_{0.1}$ causes the highest deformation level compared to the exposure of among the bigger PM. This can be seen by the deformation percentage. In this study, we investigate the type of biomass burning related to the erythrocyte deformation. As expected, the highest deformation level is obtained from the rice straw (RS) and rice husk (RH) emissions. $PM_{10}$ groups have 19%, 11%, 19%, 12%, and 19% of deformation levels for RS, TB, RH, CR, and CC. The impact of the $PM_{10}$ emission on the erythrocyte deformation, is dominated by RS and RH. A similar result that we have for $PM_{2.5}$ groups, the deformation level is obtained to 20%, 14%, 16%, 9%, and 19% for RS, TB, RH, CR, and CC, respectively. It can be seen from both the deformation level of erythrocyte caused by the $PM_{10}$ and $PM_{2.5}$ exposure shows no significant difference.

In the $PM_{0.1}$ group, the smallest deformation level is 12%, with 12 deformed cells and 91 normal cells (CR). There are 84 and 27 normal and deformed erythrocytes observed at RS, followed by 113 normal cells and 30 deformed cells at RH. There is a little increasing percentage obtained at CR compared to other PM groups (12%).

## Computational Analysis

Table 3 shows the approach results of ANN using training data ($n$ = 10) and testing data ($n$ = 5). According to this table, the most MSE in the $PM_{0.1}$ group is RS, resulting in 0.0877. The modeled deformation level of RS has 32%, 2% lower than manual counting (deformation level = 34%). The best approach can be seen in CR, showing a deformation level of 15% (MSE = 0.0081), similar to the manual counting (15%). In the $PM_{2.5}$ group, the best result is obtained from RS, with the smallest MSE value compared to other samples. The modeled deformation level is similar to the manual counting. Meanwhile, CR has the best result, resulting in an MSE value of 0.0413. It can be seen that a smaller MSE shows more precise modeling. Moreover, all results have MSE values below 0.30, indicating the good performance of ANN as the modeling tool in predicting the deformation level using manual analysis data.

According to Table 3, the LM model tests the trained data for all biomass samples and PMs. Then, each datum's error is obtained from the LM model by investigating the resulting graph's best fitting trendline. The best linearity trendline is tested using five data to get the smallest error value per target point. These comparisons are used to examine the linearity contant, $r^2$, as the comparison between manual counting and ANN approach results. A linear function shows that all PMs have fair linearity in $r^2$>0.75. The best result is $PM_{0.1}$ (Fig. 7a), showing significant linearity with $r^2$ = 0.99. It indicates that ANN works well in predicting and modeling the deformation level of erythrocytes due to biomass PM exposures. $PM_{10}$ also shows good

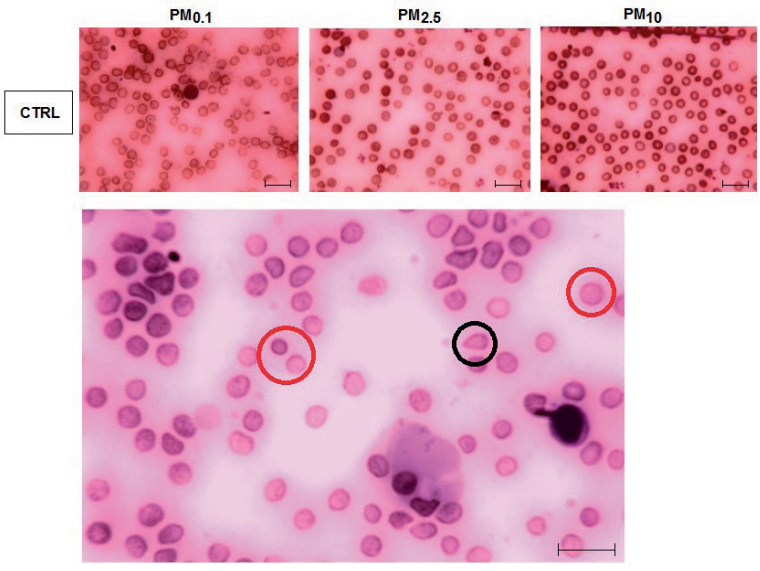


Fig. 4. The mice erythrocyte images of the control groups: RS, TB, RH, CR, and CC for all particulate matter variations (scale bar: 200 μm). Red circles = normal erythrocytes; Black circle = deformed erythrocytes.

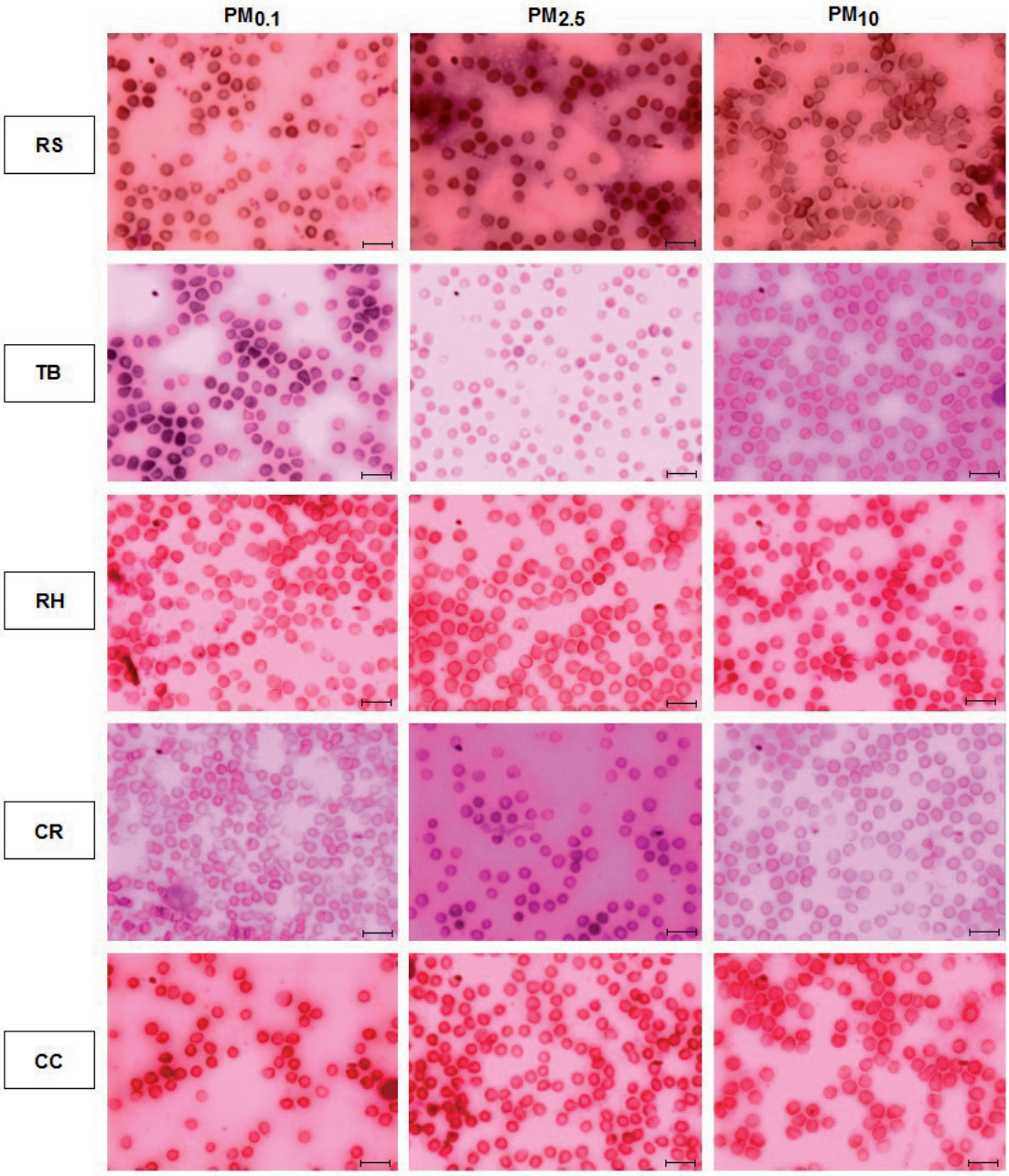


Fig. 5. The mice erythrocyte images of the exposed groups: RS, TB, RH, CR, and CC for all particulate matter variations (scale bar: 200 µm).

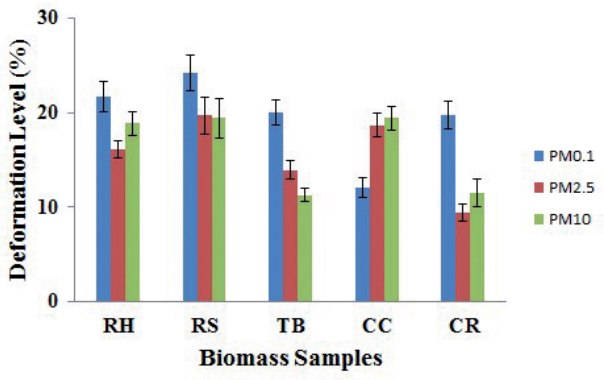


Fig. 6. Erythrocyte's deformation level from all exposed groups.

linearity, resulting in $r^2$ = 0.91 (Fig. 7c). A fair result can be seen in $PM_{2.5}$, with $r^2$ = 0.80 (Fig. 7b). These values indicate that LM can be used as the ANN modeling with better performance than the manual calculation.

This study investigates the impact of the PM exposure to erythrocyte cells, and makes a modeling with ANN (artificial neural network). For these purposes, the deformation level data are calculated from a conventional histological examination, and then the data are used as the ANN data.

In this study, we focus to analyze the relationship between the PM exposure from biomass burning and

Table 3. Deformation level comparison between ANN and manual counting results.

| $PM_{0.1}$ | | | |
|---|---|---|---|
| Samples | %DL ANN | MSE | %DL Manual |
| TB | 17 | 0.0451 | 18 |
| RS | 32 | 0.0876 | 34 |
| CR | 15 | 0.0081 | 15 |
| CC | 17 | 0.0251 | 17 |
| RH | 26 | 0.0569 | 27 |
| $PM_{2.5}$ | | | |
| Samples | %DL ANN | MSE | %DL Manual |
| TB | 14 | 0.2744 | 16 |
| RS | 12 | 0.0315 | 12 |
| CR | 10 | 0.1575 | 11 |
| CC | 14 | 0.0872 | 13 |
| RH | 9 | 0.1439 | 10 |
| $PM_{10}$ | | | |
| Samples | %DL ANN | MSE | %DL Manual |
| TB | 12 | 0.0188 | 12 |
| RS | 33 | 0.0678 | 35 |
| CR | 9 | 0.0413 | 10 |
| CC | 27 | 0.2268 | 21 |
| RH | 12 | 0.0797 | 14 |

the erythrocyte deformation of mice. The deformation was observed using a digital microscope to identify the abnormality of the cell shape. The results are compared to the control mice. Many deformed cell types are observed under random sampling, as confirmed by the previous studies [22, 32-34]. Other previous studies also confirmed deformed cells, such as saddle-shaped cells, helmet-shaped cells, sickle-shaped cells, teardrop-shaped cells, and ovalocyte [33-34]. These deformed cells have a different shape compared to the normal ones. The normal erythrocytes have a typical concave shape [22, 32-34].

According to the conventional calculation, each PM has a different deformation level in the erythrocyte. In previous studies, PM became a key point that may induce erythrocyte deformation with a different characteristic: a smaller PM is easier to deposit deeper than a bigger one [17, 35]. PM becomes a free radical that triggers ROS (reactive oxygen species) when being deposited in the body system. Then, reactive oxygen species may cause the initiation of oxidative stress [36]. ROS can cause oxidizing cellular proteins, lipids, and nucleic acids [37]. Another study supports the role of malondialdehyde (MDA) as a lipid peroxidation biomarker [38]. ROS-induced detrimental effects on the observed cells related to the decreased cytoskeletal protein content and formation of high-molecular-weight proteins. Like a chain reaction, this phenomenon leads to abnormalities and disturbances in the erythrocyte. Especially in erythrocytes, iron content and oxygen tension are related to oxidative stress, causing cell deformation [21]. As studied before, oxidative stress

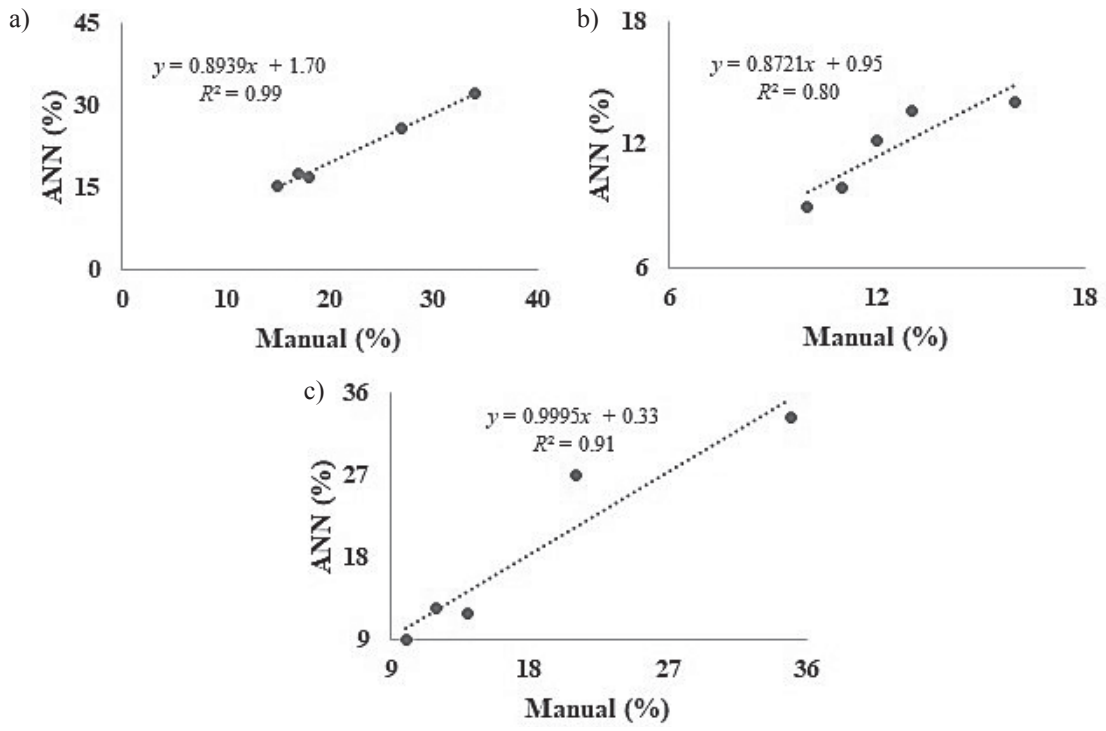


Fig. 7. Comparison between manual and ANN methods.

influences hemoglobin degradation, oxyhemoglobin oxidation, and the level of deformation [39]. The existence of strange elements such as deposited PM from biomass burning inside the cell may modulate oxidative stress via inhibiting NADPH (Nicotinamide Adenine Dinucleotide Phosphate) oxidase and other reactions production by stimulated human neutrophils [40].

As supported by the resulted data, more PM concentration has more deformation levels. It has been shown that the most PM concentration exposed to the mice causes the most deformation level. The smallest PM diameter shows the most deformation level. This study suggests new information about the impact of biomass burning exposure in the current local area may affect adverse human health. The analysis of the graphs demonstrates the probable relationship between the particulate matter diameter and the deformation level.

The focus on this research is to develop an ANN approach for predicting a deformation level. The resulting data are used as the ANN gold reference for this approach. This study shows that the developed engine generates a small number of MSE, indicating a highly accurate compared to the conventional data. As previously studied, a Levenberg-Marquardt is an ANN algorithm with the ability to have appropriate architecture, hidden neurons, and hidden layers that can be developed as a good ANN engine [27]. As a comparison in this study, there is a significant correlation between the developed engine (ANN) and the gold reference data (conventional data). This trend is shown by a linearity test with a regression coefficient ($R^2$)>0.75. These results suggest that the Levenberg-Marquardt training function has a good performance when being used as a feed-forward backpropagation network type. A small error value (MSE) shows a high similarity between the trained data and the gold reference ones [27]. This small error is highly related to the optimum layer and neuron number developed for the trained data, whether linear or non-linear approaches [27]. As supported by a previous study, iteration in the algorithm becomes a smoothing function that helps the engine to obtain the fixed-point equation and small MSE value [28]. In another word, the Levenberg-Marquardt training function has a good approach performance and can be further developed as an ANN modeling engine [29].

## Conclusion

From the study of the exposure of biomass burning particulate matter emission on the erythrocyte deformation, it is concluded that the biomass burning PM emissions have a significant impact on the erythrocyte deformation depending on the type of biomass and the particulate matter emissions. The developed ANN engine can model the erythrocyte deformation data obtained by the histological examination method with the linearity constant >0.75.

## Acknowledgments

All authors offer special thanks to all Laboratory of Air Quality and Astro Imaging, Physics Department, Brawijaya University, Indonesia.

## Conflict of Interest

The authors declare no conflict of interest.

## References

1. PHAIRUANG W., SUWATTIGA. P., CHETIYANUKOMKUL T. HONGTIEAB S., LIMPASENI W., IKEMORI F., HATA M., FURUUCHI M. The influence of the open burning of agricultural biomass and forest fires in Thailand on the carbonaceous components in size-fractionated particles. Environmental Pollution, **247**, 238, **2019**.
2. VOLKOVA L., ROXBURGH. S.H., SURAWSKI. N.C., MEYER M., WESTON C.J. Improving reporting of national greenhouse gas emissions from forest fires for emission reduction benefits: An example from Australia. Environmental Science and Policy, **94**, 49, **2019**.
3. MASON P.E., DARVELL L.I., JONES J.M., POURKASHANIAN M., WILLIAMS A. Single particle flame-combustion studies on solid biomass fuels. Fuel, **151**, 21, **2015**.
4. QUENNEHEN B., SCHWARZENBOECK A., SCHMALE J., SCHNEIDER J., SODEMANN H., STOHL A., ANCELLET G., CRUMEYROLLE S., LAW K.S. Physical and chemical properties of pollution aerosol particles transported from North America to Greenland as measured during the POLARCAT summer campaign. Atmospheric Chemistry and Physics, **11**, 10947, **2011**.
5. THEODORITSI G.N., POSNER L.N., ROBINSON A.L., YARWOOD G., KOO B., MORRIS R., MAVKO M., MOORE T., PANDIS S.N. Biomass burning organic aerosol from prescribed burning and other activities in the United States. Atmos. Environ., **241**, 117753, **2020**.
6. HUANG Y., WANG J., FU N,. ZHANG S., DU W., CHEN Y.C., WANG Z., QI M., WANG W., ZHONG Q., DUAN Y., SHEN G., TAO S. Inhalation exposure to size-segregated fine particles and particulate PAHs for the population burning biomass fuels in the Eastern Tibetan Plateau area. Ecotoxicology and Environmental Safety, **211**, 111959, **2021**.
7. XU J., JIA C., HE J., XU H., TANG Y. T., JI D., YU H., XIAO H., WANG C. Biomass burning and fungal spores as sources of fine aerosols in Yangtze River Delta, China – using multiple organic tracers to understand variability, correlations and origins. Environmental Pollution, **251**, 155, **2019**.
8. SOLAIMANI P., SAFFARI A., SIOUTAS C., BONDY S.C., CAMPBELL A. Exposure to ambient ultrafine particulate matter alters the expression of genes in primary human neurons. Neurotoxicology, **58**, 50, **2017**.

9. SHEN R., WANG Y., GAO W., CONG X., CHENG L., LI X. Size-segregated particulate matter bound polycyclic aromatic hydrocarbons (PAHs) over China: Size distribution, characteristics and health risk assessment. Science of The Total Environment, **685**, 116, **2019**.
10. WARDOYO A.Y.P., JUSWONO U.P., NOOR J.A.E. Association of diesel exhaust particle exposure with erythrocytes deformation of male mice. Applied Ecology and Environmental Research, **16** (5), 5583, **2018**.
11. TAIWO A.M. BEDDOWS D.C.S., SHI Z., HARRISON R.M. Mass and number size distributions of particulate matter components: Comparison of an industrial site and an urban background site. Science of The Total Environment, **475**, 29, **2014**.
12. WANG T., ROVIRA J., SIERRA J., CHEN S.J., MAI B.X., SCHUHMACHER M., DOMINGO J.L. Characterization and risk assessment of total suspended particles (TSP) and fine particles ($PM_{2.5}$) in a rural transformational e-waste recycling region of Southern China. Science of The Total Environment, **692**, 432, **2019**.
13. AVINO P., PROTANO C., VITALI M., MANIGRASSO M. Benchmark study on fine-mode aerosol in a big urban area and relevant doses deposited in the human respiratory tract. Enviromental Pollution, **216**, 530, **2016**.
14. GUO Y., ZENG H., ZHEN R., LI S., PEREIRA G., LIU Q., CHEN W., HUXLEY R. The burden of lung cancer mortality attributable tofine particles in China. Science of The Total Environment, **579**, 1460, **2017**.
15. CHEN Z., SALAM M.T., ECKEL S.P., BRETON C.V., GILLILAND F.D. Chronic effects of air pollution on respiratory health in Southern California children: Findings from the Southern California children's health study. Journal of Thoracic Disease, **7** (1), 46, **2015**.
16. CHEN R., HU B., LIU Y., XU J., YANG G., XU D., CHEN C. The role of ultrafine particles on adverse health effects of air pollution. Biochimica et Biophysica Acta (BBA) - General Subjects, **1860** (12), 2844, **2016**.
17. WARDOYO A.Y.P., JUSWONO U.P., NOOR J.A.E. A study of the correlation between ultrafine particle emissions in motorcycle smoke and mice erythrocyte damages. Experimental Toxicologic Pathology, **69**, 649, **2017**.
18. WARDOYO A.Y.P., JUSWONO U.P., NOOR J.A.E. Measurements of $PM_{2.5}$ motor emission concentrations and the lung damages from the exposure mice. The 2016 International Seminar on Sensors, Instrumentation, Measurement and Metrology, **3**, 99, **2016**.
19. ZHENG Z., ZHANG X., WANG J., DANDEKAR A., KIM H., QIU Y., XU X., CUI Y., WANG A., CHAN L.C., RAJAGOPALAN S., SUN Q., ZHANG K. Exposure to fine airborne particulate matters induces hepatic fibrosis in murine models. Journal of Hepatology, **63**, 1397, **2015**.
20. WARDOYO A.Y.P., JUSWONO U.P., NOOR J.A.E., A study of the correlation between ultrafine particle emissions in motorcycle smoke and mice erythrocyte damages. Exp. Toxicol. Pathol., **69** (8), 649, **2017**.
21. SHARMA P., PURI N. Data confirming murine erythrocyte opsonization and oxidative damage and live microscopic analysis of oxidatively damaged erythrocyte uptake by mast cells. Data in Brief, **20**, 1645, **2018**.
22. M. KUBÁNKOVÁ M., HOHBERGER B., HOFFMANNS J., FURST J., HERRMANN M., GUCK J., KRATER. M. Physical phenotype of blood cells is altered in COVID-19. Biophysical Journal, **120**, 2838, **2021**.
23. SHIN S., KU Y., BABU N., SINGH M. Erythrocyte deformability and its variation in diabetes mellitus. Indian Journal of Experimental Biology, **45**, 121, **2007**.
24. WARDOYO A.Y.P., JUSWONO U.P., NOOR J.A.E. How exposure to ultrafine and fine particles of car smoke can alter erythrocyte forms of male mice. Polish Journal Environmental Studies, **28**, 2901, **2019**.
25. REBY D., LEK S., DIMOPOULOS I., JOACHIM J., AULAGNIER S. Artificial neural networks as a classification method in the behavioural sciences, Behav. Processes, **40** (1), 35, **1997**.
26. BELTRAMO T., RANZAN C., HINRICHS J., HITZMANN B. Artificial neural network prediction of the biogas flow rate optimised with an ant colony algorithm, Biosyst. Eng., **143**, 68, **2016**.
27. MOSHKBAR-BAKHSHAYESH K. The ensemble approach in comparison with the diverse feature selection techniques for estimating NPPs parameters using the different learning algorithms of the feed-forward neural network, Nucl. Eng. Technol., **53**, 3944, **2021**.
28. HEMA D.D., KUMAR K.A. Levenberg-Marquardt-LSTM based efficient rear-end crash risk prediction system optimization. Int. J. Intell. Transp. Syst. Res., **20**, 32, **2022**.
29. VAEZI S.S., POORAZIZI E., TAHMOURESPOUR A., AMINSHAREI F. Application of artificial neural networks to describe the combined effect of pH, time, NaCl and ethanol concentrations on the biofilm formation of Staphylococcus aureus. Microbial Pathogenesis, **141**, 103986, **2020**.
30. WARDOYO A.Y.P., BUDIANTO A., ABDURROUF. Filtration of submicron particles from motorcycle emission using a DC low electrostatic filter. International Journal of Applied Engineering Research, **12** (8), 1725, **2017**.
31. BUDIANTO A., WARDOYO A.Y.P., MASRUROH, DHARMAWAN H.A., AND NURHUDA M. Performance test of an aerosol concentration measurement system based on quartz crystal microbalance. IOP Conf. Ser. Earth Environ. Sci., **1811 (**1), **2021**.
32. BAZANOVAS A.N., EVSTIFEEV A.I., KHAIBOULLINA S.F., SADREEV I.I., SKORINKIN A.I., KOTOV N.V. Erythrocyte: A systems model of the control of aggregation and deformability. Biosystems, **131**, 1, **2015**.
33. BUYS A.V., ROOY V.M.J., SOMA P., PAPENDORP D.V., LIPINSKI B., PRETORIUS E. Changes in red blood cell membrane structure in type 2 diabetes: A scanning electron and atomic force microscopy study. Cardiovascular Diabetology, **12**, 25, **2013**.
34. PRETORIUS E., MBOTWE S., BESTER J. Erythrocytes and their role as health indicator: Using structure in a patient-orientated precision medicine approach. Blood Reviews, **30**, 263, **2016**.
35. WARDOYO A.Y.P., JUSWONO U.P., NOOR J.A.E. Varied dose exposures to ultrafine particles in the motorcycle smoke cause kidney cell damages in male mice. Toxicol. Reports, **5**, 383, **2018**.
36. HEBBANI A. V.,VADDI D.R., DD P.P., NCH V. Protective effect of Terminalia arjuna against alcohol induced oxidative damage of rat erythrocyte membranes. Journal of Ayurveda Integrative Medicine, **12** (2), 330, **2021**.
37. GIRISH T.K., KUMAR K.A, PRASADA R.U.J.S. C-Glycosylated flavonoids from black gram husk: Protection against DNA and erythrocytes from oxidative damage and their cytotoxic effect on HeLa cells. Toxicology Reports, **3**, 652, **2016**.
38. YANG H.L., KORIVI M., LIN M-K., CHANG H C-W., WU C-R., LE M-S., CHEN W.T., HSEU Y-C.

Antihemolytic and antioxidant properties of pearl powder against 2,2′-azobis(2-amidinopropane) dihydrochloride-induced hemolysis and oxidative damage to erythrocyte membrane lipids and proteins. Journal of Food Drug Analiysis, **25**, 898, **2017**.

39. LINS P.G., PUGINE S.M.P., SCATOLINI A.M., DE MELO M.P. In vitro antioxidant activity of olive leaf extract (*Olea europaea* L.) and its protective effect on oxidative damage in human erythrocytes. Heliyon, **4** (9), 1, **2018**.
40. SARONI ARWA P., ZERAIK M.L., XIMENES F.V., DA FONSECA L.M., DA SILVA BOLZANI V., SIQUEIRA SILVA D.H. Redox-active biflavonoids from Garcinia brasiliensis as inhibitors of neutrophil oxidative burst and human erythrocyte membrane damage. J. Ethnopharmacol., **174**, 410, **2015**.